Title: Alpha oscillations for processing saliency are generated by common cortical networks in visual attention tasks spanning wide spatial and spatio-temporal scales

Abbreviated title: Temporal structure of cortical saliency processing

Author names and affiliation:

Priyanka Ghosh, Dipanjan Roy, Arpan Banerjee

Cognitive Brain Dynamics Lab, National Brain Research Centre, Manesar, Gurgaon-122052, Haryana, India

Corresponding author e-mail address:

Priyanka Ghosh (priyanka.b15@nbrc.ac.in / priyankaghoshmail@gmail.com)

Number of pages: 41

Number of figures: 5

Number of tables: 2

Number of words:

- Abstract: 250
- Significance statement: 119
- Introduction: 666
- Discussion: 1491

Conflict of interest statement: The authors declare no competing financial interests.

Acknowledgements: We thank Dr. Dipanjan Ray for his helpful comments on improving the readability of the manuscript, NBRC Core funds, and infrastructural support. PG was supported by Council of Science and Industrial Research (CSIR) fellowship (09/821(0044)/2017-EMR-I) from 03/08/2016, DR was supported by the Ramalingaswami fellowship (BT/RLF/Re-entry/07/2014) and DST-CSRI extramural grant (SR/CSRI/21/2016) and AB was supported by Ramalingaswami fellowship BT/RLF/Re-entry/31/2011) and Innovative Young Biotechnologist Award (IYBA), (BT/07/IYBA/2013).

ABSTRACT

Reorientation of attention towards unexpected salient changes around us is critical for survival. Current understanding from fMRI studies point towards a network comprising of pre-frontal cortical areas (PFC), temporo-parietal junction (TPJ) and insula being responsible for processing and reorienting attention in a myriad of tasks. However, little is known about the temporal structure of the dynamical changes that govern neural systems while reorienting attentional focus to visual stimuli operating at very fast and very slow time scales. Using a custom-designed behavioral experiment and simultaneous EEG recordings, we investigated the effect of saliency across different task conditions to see if the underlying neural signatures involved in such rapid attentional shifts change with the task conditions. Interestingly, the EEG signal power at alpha band showed near identical rise in amplitude during salient conditions for a visual search and a dynamic motion tracking task. Source reconstruction underlying the enhanced alpha activity across task conditions revealed the involvement of lateral PFC, right insula and right TPJ which are regions of the Ventral Attention Network responsible for the deployment of bottom-up attention in response to salient stimuli. The results suggested a more general role of alpha oscillations which is dependent on the task context (saliency) but not on the task complexity or goals. Employing source-level effective connectivity analysis, we observed that the posterior right TPJ receives causal influences from the anterior right TPJ. Thus, we characterized the specific roles of both these regions in salient distractor processing for the first time through an EEG study.

SIGNIFICANCE STATEMENT

Regardless of a vast body of extant literature that has linked alpha oscillations to distractor suppression, the neural implementation of this mechanism of inhibition at the level of attentional networks lacks clarity. The importance of context specificity while processing saliency and the extent to which it reflects in the alpha modulation has garnered recent interest. Through an EEG study, we see the effect of salient distractors on two visual attention tasks: 1) involving spatial complexity and 2) involving spatio-temporal complexity. The results bring forth an interesting revelation where the neural patterns of alpha enhancement vis-à-vis saliency and the underlying neural networks are completely agnostic to the task conditions, thus elucidating the specific role of alpha oscillations in perceptual processing.

INTRODUCTION

The study of the neurobiology of attention requires a detailed understanding of the resource-wise allocation of attention both in space and time, depending on the task at hand. For instance, how the brain processes information to execute a visual search over a static image is entirely different from the sensory and cognitive processing deployed in executing a task involving tracking of a dynamic stimulus (Kulikowski & Tolhurst, 1973; Stigliani, Jeska, & Grill-Spector, 2017). Where in the static scenario, there is a fixed spotlight of attention for identification of the target location to primarily deal with the "spatial complexity", a continuous object tracking is required during "temporally changing" stimulus patterns. For example, while sitting inside a moving train, constant tracking is required to read a station's name or to identify our friend from the crowd present in the station, whereas no such time-bound tracking is required when the train is stationary. Unlike a static stimulus, attention to a dynamic stimulus has limits extending over space and time, because when the speed of the stimulus increases, tracking ability decreases (P Cavanagh & Alvarez, 2005). Previous studies have reported that the minimum dwell time for attention at a fixed location is about 200 ms whereas when the focus of attention is changing along with time, a given location on the moving target's path can be selected for only brief time periods approximating to 50 ms (P Cavanagh, Battelli, & Holcombe, 2014). All these characteristics indicate that the processing of a dynamic stimulus is more complex than that of a static stimulus. Moreover, it is not just the degree of processing complexity but also the brain regions recruited and their neurophysiological underpinnings which may be entirely different for a static versus a dynamic task. Anatomical studies have shown that attention to static stimulus mostly involves contralateral brain regions whereas attention to dynamic stimulus is bilaterally organized (Battelli et al., 2001; Battelli, Pascual-Leone, & Cavanagh, 2007).

An important hallmark of attentional processing is the reorientation of attention towards unexpected salient stimuli that is critical for survival. A salient stimulus due to its 'pop-out' feature stands out from its neighbors and can rapidly capture our attention even though we do not intend to attend to it. Such stimuli reorient our attentional resources in a stimulus-driven manner to elicit what is known as 'bottom-up attention' as opposed to goal-directed 'top-down attention' (Corbetta & Shulman, 2002; Corbetta, Patel, & Shulman, 2008) that orients our attention towards a pre-decided goal or target in a task. In our study, we compare the effect of such salient stimuli between spatial and spatio-temporal visual attention tasks using electroencephalography (EEG) and behavior.

The underlying brain networks responsible for processing salient stimuli are the Ventral Attention Network/ Stimulus-driven Attention Network comprising of the anterior insula, the right temporo-parietal junction (rTPJ) and the lateral prefrontal cortical areas comprising inferior frontal/middle frontal gyri (IFG/MFG) (Vossel, Geng, & Fink, 2014; Han & Marois, 2014). The anterior insula is activated by the onset and offset of oddballs during attentional orienting/reorienting and is hypothesized to be associated with the capture of focal attention by salient stimuli (Menon & Uddin, 2010). On the other hand, fMRI studies have shown that the lateral pre-frontal cortex (lPFC) plays a role in the integration of sensory information between the anterior insula and TPJ (Kubit & Jack, 2013). Few studies have reported the involvement of both the left and the right TPJ and its role in reorientation in response to salient stimuli (Krall et al., 2015; Carter & Huettel, 2013; Decety & Lamm, 2007). Nonetheless, the functional role of TPJ is highly debated and so is its location, due to an unusually high degree of inter-individual variability in its anatomical structure (Van Essen, 2005; Caspers et al., 2006). Although multiple fMRI studies have evaluated the role of TPJ in context of saliency processing, as per our knowledge the present EEG study is the first to show causal influences among the constituent cortical loci involved in the deployment of bottom-up attention.

METHODS

Participants

22 healthy human volunteers (11 females and 11 males) aged between 21-29 (mean = 26.9, SD = ±2.15) years were recruited for the study. All participants had University degrees or higher; were right handed (indexed by laterality score according to the Edinburgh handedness questionnaire); reported normal or corrected-to-normal vision; and declared no history of neurological or psychiatric disorders. The participants were requested to avoid the intake of any stimulant or medication (e.g., coffee, sedatives etc.) before coming for the experiment. The study was carried out following the ethical guidelines and prior approval of the Institutional Review Board of National Brain Research Centre, India which conforms to the standard set by the Declaration of Helsinki. Written informed consent was obtained from all participants before the commencement of the experiment and they were remunerated for the time of their participation.

Rest block

Before starting with the experimental task, five minutes of eyes open resting-state EEG data were collected from the participants. During this period, a blank black screen was presented on the monitor. The participants were asked to relax or think at free will while viewing the monitor screen placed before them. They were requested to make minimal head, body and eye movements.

Stimulation blocks

All the participants performed two visual attention-based tasks which incorporated two stimulus conditions: static and dynamic **(Figure 1)**. The entire experiment was divided into 16 blocks (8 blocks of each stimulus condition). Each block was presented in a random order

during the experiment but was never repeated. Both the visual tasks had three categories of trials: 'Without Saliency Trials' **(WT)**, 'Saliency Trials' (**ST**) and 'Neutral Trials' (**NT**). The presentation order of the three categories was randomized in each block. The participants were not aware of the categorization in trials and were instructed only about the respective goals of the static and dynamic tasks before the experiment.

The NT served as a control to the participants' attention. They were introduced to keep a check if the participants were attentive throughout the experiment and were just not making random responses. The NT were designed to give an impression of the most difficult trials to the participants, which if attended, were expected to produce the longest reaction times. The distribution of trials within a block for both the static and dynamic visual tasks is given in **Table 1.**

Inter-stimulus intervals (ISI) between successive trials were randomly drawn from a uniform distribution with values ranging between 500 ms and 1500 ms (mean = 1000ms) in which a blank black screen was presented to avoid any saliency-related effects due to central fixation.

Stimulus presentation and behavioral response collection were done using Neurobehavioral Systems (NBS) Presentation software. Participants viewed the stimuli on a 21'' LED screen (1280 X 1024 pixels) with a 60 Hz refresh rate placed on a 74-cm-high desktop. The center of the screen was placed within 10–20° of the participant's line of sight, at a 60–70 cm distance. The stimuli were presented on a black background over which the static stimulus covered an area of 20 X 20 cm on the screen whereas the diameter of the aperture in the dynamic stimulus was 20 cm.

Dynamic stimulus: The dynamic stimulus viewing task was a four-alternative forced choice (4-AFC) task. The stimuli were designed using Psychtoolbox-3 in MATLAB R2016b and were exported as videos with a frame rate of 60 Hz. The participants were presented these videos

which consisted of white-colored equal-sized randomly moving dots where, a proportion of dots moved in a particular direction because of a certain coherence assigned to them. The coherence of the dots was kept at 0.6 for all the trials, which means that out of 100 dots, 60 dots moved in one specific direction and the other 40 moved in random directions, uniformly distributed over 0-360 degrees. The speed of motion of all the dots was kept constant across all trials. The participants were instructed to identify the net direction of the moving dots which could either be left/right/up/down and respond using the respective arrow keys on the keyboard. Each video was presented for 2000 ms. The goal in the task was the same for both WT and ST, with the only difference in the latter being the emergence of a salient dot at a timestamp of 150 ms from the onset of the trial, moving randomly within the same aperture as the other dots. The 150 ms latency was decided with the purpose of creating an interference in the decision-making process (Teichert, Grinband, & Ferrera, 2016) of the participant while doing the goal directed task. The experimental schematic is illustrated in **Figure 1.**

Static stimulus: The static stimulus consisted of a two-alternative forced choice (2-AFC) task. The participants were presented with two similar pictures on the screen, successively. Each picture pair made up one trial and was randomly selected from a pool of twenty such picture pairs. Thirty such picture pairs were presented in one block. The pictures were naturalistic images (from both indoor and outdoor settings; no faces included) captured using a 16 MP camera keeping the settings same for all images. Using Adobe Photoshop CC 2015.5, a white-colored '+' shape (size 1/800th of the image) was added to all the images at random positions. Multiple copies of a single image with '+' shape at different positions were created such that there was no image and '+' position memory association. Each picture was presented for 2000 ms. This was a visual search task where the participants had to search for the white-colored '+' shape in both the pictures and report its change in position in the second picture with respect to the first picture. For convenience, the participants were advised to imagine a vertical line

bisecting the screen into left and right halves. They were instructed to press the upward arrow key if the '+' sign moved to the same half of the screen in the second picture, i.e, change in position was on the same side of the imaginary line; and to press the downward arrow key if the '+' sign changed its position and moved to the other half of the screen i.e, from the left half to the right half or vice versa. The goal in the task was same for WT and ST, with the only difference in the latter being the introduction of a salient ('pop-out') object in the second picture at any random position. An example of one such stimulus is presented in **Figure 1.**

EEG Data Acquisition

Behavioral and EEG data were acquired in the EEG recording room where ambient noise, light, and other interferences were strictly controlled during the experiment to the same levels for all recording sessions. A Neuroscan EEG recording and acquisition system (Scan 4.3.3 & Presentation), which included an elastic cap (EasyCap) with 64 Ag/AgCl sintered electrodes and amplifier (SynAmps2), was used. The 64-channel EEG signals were recorded according to the International 10–20 system of electrode placement. Cz was the reference electrode, grounded to AFz and the impedance of all channels was kept below 10 kΩ. The data were acquired at a sampling rate of 1000 Hz. A Polhemus Fastrak system was used to record the 3D location of electrodes using a set of fiducial points (Cz, nasion, inion, left and right pre-auricular points) while the EEG cap was placed on the participant's head.

Behavioral Data Acquisition

All the responses were made on a computer keyboard using left/right/up/down arrow keys and were recorded through the NBS Presentation software by receiving triggers at keyboard

presses. Before the experiment, the participants were instructed to watch the stimulus carefully before making any response. They were asked to be as fast and as accurate as possible and respond to an ongoing trial before it's offset. A blank screen followed by the subsequent trial appeared automatically after the offset of the ongoing trial, regardless of whether the participants had responded or not. They were also asked to respond to all the trials. If more than one response was made for a trial, only the first response was considered for further analysis. A rest period was allowed after every block, with the participant deciding the length of the rest period to maintain minimum fatigue.

EEG Data Preprocessing

For both the static and the dynamic tasks, pre-processing steps and analysis pipeline were identical. All the pre-processing steps were done with the EEGLAB toolbox (Delorme & Makeig, 2004) and custom-written scripts in MATLAB (www.mathworks.com).

Raw EEG data from all the participants were imported using EEGLAB toolbox (Delorme & Makeig, 2004) following which they were first filtered using a band-pass filter of 0.1-80 Hz followed by a notch filter between 45-55 Hz to eliminate line noise at 50 Hz. Post filtering, the data were visually inspected and the trials with any abnormal or noisy segments (jitters with very large amplitudes) were removed. Data of two participants were discarded at this step due to very noisy recordings. Next, the filtered data were re-referenced to the common average. Epochs of 1000 ms post salient stimulus onset were extracted using trigger information and were sorted from WT, ST and NT categories. Trial-by-trial detrending of each epoch category was performed to remove linear trends from the signal. To further remove ocular, muscular and electrocardiograph artifacts, a threshold of ±75μV was set and trials with a magnitude

beyond this threshold at any time-point were rejected from all the channels. Overall, about 70% of the trials for each task condition from each subject were preserved after artifact rejection.

Behavioral Analysis

The reaction times and accuracies of all the trials were calculated. Since attention is a key component in our experiment and any form of distraction (internal/external) could shift attention away from the task, blocks with response accuracies less than 70% (less than 6% of all blocks) were excluded from further analysis. To decrease the number of false positives and minimizing chances of including responses made without the involvement of attention, all incorrect trials including the skipped trials were also excluded. Data from one participant were discarded due to very poor performance specifically in dynamic task trials. To rule out the possibility of incorrect responses being made because of a specific directional bias in any participant, we computed the percentage of incorrect responses for each direction and found that it was nearly the same for all directions in each individual.

From the remaining 19 participants, the reaction times of the correct trials were sorted and averaged across all the participants for both static and dynamic tasks. The reaction time was the duration from the onset of the stimulus till the participant hit the response button. For the NT, any response was considered as correct.

Spectral Analysis

To understand the neural correlates of the behavior and hence, the processing of saliency by the brain, we looked at the constituent frequencies from 0.1-80 Hz in the individual trial categories of both the tasks. Power spectrum analysis was performed on the EEG time series

data for the 19 participants. To ensure an equal contribution of trials from each participant, the number of trials from the participant with the minimum number of remaining trials after artifact rejection was chosen for further analysis. Those many trials were randomly sampled and extracted from all the three categories for each participant. Since 35 was the minimum number, we had a total of 665 (19*35) trials from each category in both static and dynamic tasks.

The analysis scheme was designed in a way that could tease out the effect of the salient distractor while doing the goal-directed task and therefore, a time window of 1000 ms from the onset of saliency was considered (timestamps were matched accordingly for WT and NT). Using the EEG time-series data, we calculated the power spectral density for each trial corresponding to all the 64 channels using the multi-taper method (mtspectrumc.m) provided by Chronux toolbox (Bokil, Andrews, Kulkarni, Mehta, & Mitra, 2010). A standard multi-taper FFT was used that applied 5 Slepian tapers to each window (time bandwidth product = 3). Sampling frequency was kept at 1000 Hz and frequencies were estimated between 0.1 to 80 Hz.

Source Reconstruction using individual T1 MRI images

To localize the sources of the alpha band activity, we applied a current density technique: exact low-resolution brain electromagnetic tomography (eLORETA) implemented by the MATLAB-based Fieldtrip toolbox. eLORETA (Pascual-Marqui, 2007) is a weighted minimum norm inverse solution that provides exact localization with zero error in the presence of measurement and structured biological noise. We first created the forward models of individual participants using their respective T1-weighted structural MRI images (MPRAGE) collected from a Philips Achieva 3.0 T MRI scanner using the following acquisition parameters: TR = 8.4 ms, FOV = 250 X 230 X 170, flip angle = 8 degrees, and fiducials marked at nasion, left

and right pre-auricular points with Vitamin E capsules. The origin of all the T1 images was set to the anterior commissure using SPM 8 before generating individual head models. Using Boundary Element Method (BEM), the brain was segmented into a mesh/grid based on the geometrical and tissue properties of the brain. The Polhemus data with the electrode locations of individual subjects, was then fitted over these individual head models co-registered to the MRI fiducial points to create the leadfield matrix corresponding to each participant. For a frequency-domain source analysis, the cross-spectral density (CSD) matrix, which contains the cross-spectral densities for all sensor combinations, was computed for individual participants from the Fourier transformed data for the alpha frequency band (8-12 Hz).

Using the CSD matrix and the lead field matrix, a spatial filter was calculated for each grid point. By applying this spatial filter to both the trial conditions (WT and ST) separately, the power estimate for each grid point was obtained. For calculating the source power, a common filter approach was used to ensure that the differences in source power across the two trial conditions were actually because of differences in the brain activity and not because of differences in the filter output (which might arise due to variations in the signal-to-noise ratio and subsequently varying CSD matrices) in the two trial conditions (WT and ST). Using this common inverse filter, the net source power was computed for each participant and the individual grids were interpolated with their respective T1 weighted images followed by normalization over a common Colin 27 brain template. The statistical threshold was set at 99% significance level to define activated sources of alpha enhancement.

Source Time-series Reconstruction

From the thresholded grid points, we reconstructed the time series for the activated ROIs at the source level by multiplying the spatial filter with the artifact rejected time-series data

using common electrode placements for all individuals computed by taking the average of their normalized 3-D locations. The projection of the filter onto the EEG time series data for each task condition yielded 3 source dipole time-series with their orientations along the x, y and z directions. Since the interpretation of results becomes difficult while dealing with three dipole orientations, the time-series were projected along the strongest dipole direction. This was done by determining the largest (temporal) eigenvector corresponding to the first singular value. Using these reconstructed time series, connectivity analyses were done for each task condition to look for effective connectivity between the sources involved in processing saliency.

Effective Connectivity Analysis

To understand the directional interactions between the sources, effective connectivity was calculated using conditional Granger Causality in the time domain using a Causality Estimating Software (https://www.dcs.warwick.ac.uk/~feng/causality.html). This software uses a time-varying Granger Causality approach catered to deal with non-stationary time series of EEG/MEG data, unlike the traditional Granger Causality methods that fit a time-invariant multivariate autoregressive model (MVAR) to the time series.

The reconstructed time-series from each participant was treated as a trial, leading to reconstruction of 19 trials from 19 participants. One participant's data from the dynamic stimulus was removed as the reconstructed time series data was very noisy. To further reduce non-stationarity, all the reconstructed time series were bandpass filtered between 5-45Hz to minimize the effects of evoked potentials. A connectivity matrix was created between all the nodes (7 X 7 for dynamic stimulus and 5 X 5 for static stimulus). The time series data for each node was subjected to 50 rounds of bootstrapping from which the mean Granger causality value

for each causation combination was obtained. To test the statistical significance of these values, a 95% confidence interval was generated empirically from a null distribution by random permutation of the time series across all the nodes and trials for 50 times. Subsequently, Granger causality estimates were obtained for these 50 iterations, and the mean and the standard deviation were computed from the GC values to compute the confidence interval at 95% significance.

RESULTS

Behavioral responses to saliency in static and dynamic tasks

The mean and standard error of the mean of the reaction times of all the trial categories NT, WT and ST are shown in **Figure 2** for dynamic and static tasks. Statistical significance was computed using Wilcoxon rank-sum test where the null hypothesis of no significant difference between reaction times of any two categories in a task condition was tested at 95% confidence level. The reaction times showed a significant difference (NT>WT at $p<0.0001$, NT>ST at $p<0.0001$ and ST>WT at $p=0.012$ in dynamic task; NT>WT at $p<0.0001$, NT>ST at $p<0.0001$ and ST>WT at $p<0.0001$ in static task) between each trial category within a task and followed a similar pattern of reaction time relationship in both the tasks which was: NT >ST > WT.

Alpha modulations associated with the reorientation of attention towards salient distractor in static and dynamic tasks

The power spectra were calculated for WT, ST and NT of all the participants trial-by-trial, which was subsequently averaged and collapsed across all the 64 sensors for both the task conditions: dynamic and static. **Figure 3** compares the normalized power spectra for ST, WT and NT. Though all the trial categories in a task followed the same pattern of power spectra, the power of the alpha frequency band (8-12 Hz) was higher for the ST as compared to the WT and the NT. Interestingly, this pattern was seen in case of both dynamic and static stimuli. To test out the statistical significance of the increased alpha power, we employed a non-parametric Wilcoxon rank-sum test which revealed that alpha power significantly increased in ST as compared to WT ($p=0.002$) and NT ($p<0.001$) for the static stimulus condition between 8 to 11 Hz at 95% confidence level. Similarly, in the dynamic stimulus condition, there was a significant increase ($p = 0.04$) in the alpha power of ST as compared to WT between 8 to 11

Hz. The increase of power in ST as compared to NT was however, not that significant ($p = 0.06$). To verify the robustness of this alpha enhancement pattern and find the peak alpha frequency, we employed a detrending method and compared the alpha power spectra of NT, WT and ST conditions. Here, we modeled the 1/f trend of the log-transformed power spectrum and subtracted this trend from our original power spectrum data. This detrended power spectrum was then plotted for the entire alpha frequency range between 7 to 14 Hz. Interestingly, the enhanced power of ST had a peak frequency at 10 Hz for both the static and the dynamic tasks (**insets to Figure 3**).

The topoplots for dynamic and static stimulus processing conditions were plotted (**insets to Figure 3**) for the peak alpha frequency (~10 Hz) using the formula of alpha modulation index (AMI) (Sokoliuk et al., 2019).

$$Net\ increase\ in\ alpha\ power\ in\ ST = \frac{Sensor\ power\ of\ ST - Sensor\ power\ of\ WT}{0.5 * (Sensor\ power\ of\ ST + Sensor\ power\ of\ WT)} \quad (1)$$

Sensors Fz, F3, F5, F7, FC5, FT7, CP5, TP7, CP4, CP6, P4, P6, P8, PO4, PO6, PO8 and O2 showed the maximum increase in their peak alpha powers at 10 Hz in ST in the dynamic task. Similarly, sensors AF3, F1, F3, F5, F6, F7, FC5, FT7, T7, TP7, CP2, CP4, CP6, TP8, P2, P4, P6, PO3, PO4 and PO6 showed the maximum alpha power increase at 10 Hz in the static task. Overall, in both the tasks, enhanced alpha power concentrated around the centro-parietal, parietal, parieto-occipital and temporo-parietal sensors on the right; and on the frontal, fronto-central and temporo-parietal sensors on the left.

The underlying sources of saliency related alpha activity in static and dynamic tasks

The underlying sources responsible for the enhanced alpha power in ST with respect to WT were calculated using the same formula of alpha modulation index (AMI) at the peak alpha

frequency (~10 Hz) after computing the individual sources for ST and WT using eLORETA (as described in methods).

The relative difference in source powers during ST and WT conditions produced the residual source powers. We argue that the dynamic or static task-specific information was thus negated and the residuals reflect the effect of saliency only. The source powers for all participants were grand-averaged and tested for statistical significance. The grid points that survived 99th percentile threshold, were considered as significant sources of activation in response to salient distractors. For the purpose of plotting, the source coordinates in the 3-D voxel space were projected to a surface plot as represented in **Figure 4** using customized MATLAB codes. Spurious activations towards the center of the brain arising from noise were removed by masking the grid points deep inside the brain with an ellipsoid of optimum radii centered at the anterior commissure.

The underlying sources of alpha enhancement in the dynamic task were the left and the right anterior temporo-parietal junction (supramarginal gyrus), right posterior temporo-parietal junction (angular gyrus), the right insula, the lateral prefrontal cortex and regions from the left and the right visual cortex.

The sources corresponding to alpha power enhancement in static task were the left and the right anterior temporo-parietal junction (supramarginal gyrus), the right insula, the right lateral prefrontal cortex (including the inferior frontal gyrus) and regions from the right visual cortex.

Since the reconstructed time series obtained using the thresholded sources consisted of very few (~1000) grid points from the entire brain, we reconstructed the sources again with a lower threshold (98th percentile), to get more number of grid points. Even though the number of grid points increased upon lowering the threshold, the anatomical landmarks corresponding to source locations did not show much difference overall. Further, using k-means clustering, these

sources were classified into nodes based on the centroid of the sources. Sources corresponding to the dynamic task were classified into 7 nodes whereas for the static task, they were classified into 5 nodes. All the regions corresponding to these nodes with their respective coordinates (approximated to the nearest Brodmann areas) have been listed in **Table 2**.

The observed alpha power enhancement during dynamic stimulus processing correspond to two sub-regions of the right TPJ: the anterior and the posterior right TPJ. To further confirm those were not just two clusters obtained from a single big region due to a limitation of the clustering algorithm, we calculated the Euclidean distance between the right anterior and posterior TPJ based on their coordinates, which was equal to 28.80 mm, which showed that the two sub-regions were considerably far apart to be considered as two distinct ROIs. We have also checked the consistency of these two sources at an individual subject level. In total, 18 out of the 19 participants showed activations in both the anterior and posterior TPJ at 99^{th} percentile threshold while the remaining one participant exhibited the same upon further lowering the threshold to 95^{th} percentile.

Effective brain network connectivity while processing saliency in static and dynamic tasks

Source time series computed from 7 sources in dynamic stimulus and 5 sources in static stimulus processing conditions were subjected to Granger causality (GC) analysis to understand the directional influence between the sources. Out of all the significant functional connections (95% confidence interval) from a total of 42 possible connections during dynamic stimulus processing and 20 such connections during static stimulus processing, we chose to focus on the top 50 percentile connections that had a relatively high GC as illustrated in **Figure 5**.

Granger causality revealed the following causal influences:

Right Visual Area → Right Insula, Right Visual Area → Right anterior TPJ, Right Visual Area → Right lateral PFC, Right Insula → Right posterior TPJ, Right anterior TPJ → Right posterior TPJ, Right anterior TPJ → Left Visual Area for dynamic viewing and the following ones: Right Visual Area → Right Insula, Right Visual Area → Right anterior TPJ, Left anterior TPJ → Right anterior TPJ for static viewing conditions.

The brain networks were visualized using BrainNet Viewer (Xia, Wang, & He, 2013). Overall, there is clearly a right hemispheric dominance of network interactions during saliency processing in both static and dynamic tasks.

DISCUSSION

Our results show that the underlying neural oscillations mediating the activation of the salience driven attentional sources (mostly regions of the Ventral Attention Network) leading to the reorientation of attention from a goal-directed task come from the alpha frequency band (8-12 Hz).

Increased response times in salient trials as an outcome of two neural sub-processes

The behavioral results indicate that the salient distractor in the ST might have contributed to the increased latency in reaction time (Noonan et al., 2016). This can be attributed to both the 'pop-out' property of the salient distractor which leads to attentional reorientation towards it, as well as the orientation back to the goal driven task. These two processes are absent in WT and hence they have a comparatively shorter reaction time. Since these results indicate that the salient distractor has been attended in ST, it is imperative that it is a consequence of cortical information processing. However, the NT, which had no possible correct responses and yet required a goal directed attention, resulted in higher RTs possibly reflecting the role of increased cognitive load/ task complexity. Hence, it is important to characterize whether the neural dynamics corresponding to salient stimulus is due to an attentional shift alone or attention combined with task complexity.

Alpha power enhancement related to saliency trials invariant across task conditions

One view regarding the role of alpha oscillations is that an increase in alpha power reflects distractor suppression, whereas a decrease in alpha power reflects release from suppression (Fries, Reynolds, Rorie, & Desimone, 2001; Fu et al., 2001; Jensen & Mazaheri, 2010; Klimesch, 2012). Also well-established is the fact that increased parietal alpha synchrony (8–

12 Hz) in one hemisphere is associated with reduced attention in the contralateral visual field such that the distractor can possibly be ignored (Foxe, Simpson, & Ahlfors, 1998; Worden, Foxe, Wang, & Simpson, 2000; Foxe, Simpson, Ahlfors, & Saron, 2005; Snyder & Foxe, 2010; Banerjee, Snyder, Molholm, & Foxe, 2011; Zumer, Scheeringa, Schoffelen, Norris, & Jensen, 2014; Liu, Bengson, Huang, Mangun, & Ding, 2014; Feng, Störmer, Martinez, McDonald, & Hillyard, 2017).

In accordance to these findings, our power spectral density results reveal there was a significant enhancement in the alpha power of ST as compared to WT and NT with no significant changes between WT and NT. Interestingly, the pattern of enhancement was very similar for the static and dynamic stimulus conditions in terms of the peak frequency (~10Hz) and the magnitude of the enhanced power. This pattern of similarity is suggestive of a more task-independent role of alpha while processing salient distractors, that does not depend on the task condition *per se* but is mostly a consequence of the context of the task, which in this case is saliency. Furthermore, alpha power levels for WT and NT didn't show any significant difference, though their reaction times were significantly different. This rules out the possibility of alpha increase stemming from task complexity. Nonetheless, to explicitly explore the trend we computed the peak alpha power of all participants and checked their correlation with reaction times, and not surprisingly no significant differences were observed.

In line with our work, a recent study showed that distraction suppression through alpha oscillations does not depend on the spatial location of the target through an auditory spatial pitch discrimination task (Wöstmann, Alavash, & Obleser, 2019). In real life situations however, we constantly interact with a variety of stimulus conditions and it is important to characterize how is distractor suppression modulated with the various stimulus conditions so that a neural marker for saliency can be established.

Common sources of alpha activity to process saliency across dynamic and static task conditions

The topoplots at peak alpha power indicated the presence of a possible overlap in the right centro-parietal and parieto-occipital regions of cortex for processing saliency related information and guided us to further delve into the source space. Source reconstruction results revealed that most of the sources were overlapping in the two task conditions. The right insula, the right anterior temporo-parietal junction (TPJ), the right lateral prefrontal cortex and the right visual association areas showed source activations underlying alpha enhancement in both static and dynamic stimulus conditions. The aforementioned regions have been extensively shown to be involved in the processing of salient stimuli in previous fMRI studies and are also a part of the Ventral Attention Network (VAN) which is mostly right lateralized (Schuwerk, Schurz, Müller, Rupprecht, & Sommer, 2017; Eddy, 2016; Krall et al., 2015; Han & Marois, 2014). TPJ has been shown to have a role that kicks in later during stimulus driven attentional reorientation and in the integration of internal representations of task context with stimulus and response expectations (Geng & Vossel, 2013). An additional observation from our source reconstruction results was the behavioral relevance specific posterior TPJ activation in the dynamic stimulus condition that is not seen in the static task condition. Extant studies (Corbetta & Shulman, 2002; Corbetta et al., 2008) suggest that the right TPJ shows activation in response to salient distractors that are only behaviorally relevant (Huang, Tang, Sun, & Luo, 2018). A salient distractor can be considered to be behaviorally relevant if it shares features with the target of the task. The salient distractor in the dynamic task condition was hence behaviorally relevant to the task (differently sized/ colored dot amidst other dots) whereas in the static task condition it was not (complex naturalistic objects as opposed to a target which was a basic

geometrical shape '+'). Using diffusion-weighted imaging tractrography–based parcellation, Mars and colleagues demarcated TPJ into 3 distinct sub regions: anterior TPJ (supra-marginal gyrus), posterior TPJ (angular gyrus) and the dorsal TPJ (middle part of the inferior parietal lobule) (Mars et al., 2012; Carter & Huettel, 2013; Geng & Vossel, 2013). The first two sub-regions are consistent with our source reconstruction results. Similar studies by Kubit and Jack (2013), identified these TPJ sub-regions to be associated with target detection, oddball identification and mentalization/ social cognition, respectively.

Directional causality from anterior to posterior rTPJ for behaviorally relevant salient stimuli

Identification of the almost common set of brain areas underlying alpha enhancement across dynamic and static stimuli warrants the understanding of the causal relationships among the candidate nodes. Granger Causality analysis on dynamic viewing condition revealed that the posterior TPJ is driven by the anterior TPJ. Posterior TPJ has been shown to be associated with identification and evaluation based processes in oddballs (Kubit & Jack, 2013). The anterior TPJ on the other hand, has exclusively been reported to be a part of the ventral attention network (VAN) and is responsible for the reorientation of attention whenever faced with a salient distractor (Rennig, Himmelbach, Huberle, & Karnath, 2015; Igelström, Webb, & Graziano, 2015), which is perhaps a transient process involved in the switch of attention from the task goals to a salient distractor (Han & Marois, 2014). If the salient distractor is behaviourally inconsequential, based on comparison of sensory information to internal representations (Krall et al., 2015), attention is oriented back to the task at hand. Based on our connectivity results, we propose that a behaviorally relevant salient distractor (as in the case of dynamic task) is further processed in the posterior rTPJ which evaluates the contents of the

526 distractor and subsequently plays a gating role in driving the attentional requirements. Thus,
527 the behaviourally relevant distractor is prioritized over a behaviourally irrelevant one at the
528 stage of anterior TPJ such that the latter is not forwarded for further processing. On this view,
529 a recent study has reported that the TPJ does not directly compute the relevance of a stimulus
530 feature, but modulates its response to stimuli according to the top-down biasing of signals to
531 control the engagement of attention to potentially distracting information that is behaviorally
532 relevant to the task (Pedrazzini & Ptak, 2019).

533

534 **Posterior rTPJ has a decisive role in reorientation of attention**

535 Finally, as a prospective avenue for future research, we speculate that characterizing the various
536 sub-regions of TPJ will probably be of critical importance to neuroscience in order to
537 understand the subtle variations of attentional processing, both for spatial as well as spatio-
538 temporally enriched stimuli. Although, various studies have explicitly mentioned about the
539 sub-regions of TPJ in this regard, we would like to go a step forward and propose that the
540 posterior TPJ receives top-down biasing signals from the anterior TPJ that help modulate our
541 responses based on the relevance of a distractor to a putative task. We note that such a crucial
542 claim over the spatial anatomy of a sub-region just based on an EEG study comes with several
543 limitations, nonetheless, underpinning the transient changes in neural dynamics associated with
544 the processing of saliency and the attentional reorientation that follows, require temporal
545 precision which is difficult to achieve through other neuroimaging techniques like fMRI.
546 Recently, some evidences have shown that the detection of very focal activations for cortical
547 sources may be possible using EEG source reconstruction (Halder, Talwar, Jaiswal, &
548 Banerjee, 2019).

549

REFERENCES

Banerjee, S., Snyder, A. C., Molholm, S., & Foxe, J. J. (2011). Oscillatory alpha-band mechanisms and the deployment of spatial attention to anticipated auditory and visual target locations: Supramodal or sensory-specific control mechanisms? *Journal of Neuroscience*, *31*(27), 9923–9932. https://doi.org/10.1523/JNEUROSCI.4660-10.2011

Battelli, L., Cavanagh, P., Intriligator, J., Tramo, M. J., Hénaff, M.-A., Michèl, F., & Barton, J. J. S. (2001). Unilateral Right Parietal Damage Leads to Bilateral Deficit for High-Level Motion. *Neuron*, *32*(6), 985–995. https://doi.org/10.1016/S0896-6273(01)00536-0

Battelli, L., Pascual-Leone, A., & Cavanagh, P. (2007). The 'when' pathway of the right parietal lobe. *Trends in Cognitive Sciences*, *11*(5), 204–210. https://doi.org/10.1016/j.tics.2007.03.001

Bokil, H., Andrews, P., Kulkarni, J. E., Mehta, S., & Mitra, P. P. (2010). Chronux: A platform for analyzing neural signals. *Journal of Neuroscience Methods*, *192*(1), 146–151. https://doi.org/10.1016/j.jneumeth.2010.06.020

Carter, R. M., & Huettel, S. A. (2013). A nexus model of the temporal-parietal junction. *Trends in Cognitive Sciences*, *17*(7), 328–336. https://doi.org/10.1016/j.tics.2013.05.007

Caspers, S., Geyer, S., Schleicher, A., Mohlberg, H., Amunts, K., & Zilles, K. (2006). The human inferior parietal cortex: Cytoarchitectonic parcellation and interindividual variability. *NeuroImage*, *33*(2), 430–448. https://doi.org/10.1016/j.neuroimage.2006.06.054

Cavanagh, P, & Alvarez, G. (2005). Tracking multiple targets with multifocal attention. *Trends in Cognitive Sciences*, *9*(7), 349–354. https://doi.org/10.1016/j.tics.2005.05.009

Cavanagh, P, Battelli, L., & Holcombe, A. O. (2014). *Dynamic attention Introduction: Tracking Events as They Unfold in Time*. Retrieved from

574 https://cavlab.net/MyRWResources/MyPDFs/PDF2014/Cavanaghetal2014.pdf

575

576 Corbetta, M., Patel, G., & Shulman, G. L. (2008). The Reorienting System of the Human Brain:
577 From Environment to Theory of Mind. *Neuron*, *58*(3), 306–324.
578 https://doi.org/10.1016/j.neuron.2008.04.017

579 Corbetta, M., & Shulman, G. L. (2002). Control of Goal-Directed and Stimulus-Driven
580 Attention in the Brain. *Nature Reviews Neuroscience*, *3*(3), 215–229.
581 https://doi.org/10.1038/nrn755

582 Decety, J., & Lamm, C. (2007). The Role of the Right Temporoparietal Junction in Social
583 Interaction: How Low-Level Computational Processes Contribute to Meta-Cognition. *The*
584 *Neuroscientist*, *13*(6), 580–593. https://doi.org/10.1177/1073858407304654

585 Delorme, A., & Makeig, S. (2004). EEGLAB: An open source toolbox for analysis of single-
586 trial EEG dynamics including independent component analysis. *Journal of Neuroscience*
587 *Methods*, *134*(1), 9–21. https://doi.org/10.1016/j.jneumeth.2003.10.009

588 Eddy, C. M. (2016). The junction between self and other? Temporo-parietal dysfunction in
589 neuropsychiatry. *Neuropsychologia*, *89*, 465–477.
590 https://doi.org/10.1016/J.NEUROPSYCHOLOGIA.2016.07.030

591 Feng, W., Störmer, V. S., Martinez, A., McDonald, J. J., & Hillyard, S. A. (2017). Involuntary
592 orienting of attention to a sound desynchronizes the occipital alpha rhythm and improves
593 visual perception. *NeuroImage*, *150*, 318–328.
594 https://doi.org/10.1016/j.neuroimage.2017.02.033

595 Foxe, J. J., Simpson, G. V., & Ahlfors, S. P. (1998). Parieto-occipital ~10 Hz activity reflects
596 anticipatory state of visual attention mechanisms. *NeuroReport*, *9*(17), 3929–3933.
597 https://doi.org/10.1097/00001756-199812010-00030

598 Foxe, J. J., Simpson, G. V., Ahlfors, S. P., & Saron, C. D. (2005). Biasing the brain's attentional
599 set: I. Cue driven deployments of intersensory selective attention. In *Experimental Brain*
600 *Research* (Vol. 166, pp. 370–392). https://doi.org/10.1007/s00221-005-2378-7

601 Fries, P., Reynolds, J. H., Rorie, A. E., & Desimone, R. (2001). Modulation of oscillatory
602 neuronal synchronization by selective visual attention. *Science*, *291*(5508), 1560–1563.
603 https://doi.org/10.1126/science.1055465

604 Fu, K. M. G., Foxe, J. J., Murray, M. M., Higgins, B. A., Javitt, D. C., & Schroeder, C. E.
605 (2001). Attention-dependent suppression of distracter visual input can be cross-modally
606 cued as indexed by anticipatory parieto-occipital alpha-band oscillations. *Cognitive Brain*
607 *Research*, *12*(1), 145–152. https://doi.org/10.1016/S0926-6410(01)00034-9

608 Geng, J. J., & Vossel, S. (2013). Re-evaluating the role of TPJ in attentional control: Contextual
609 updating? *Neuroscience & Biobehavioral Reviews*, *37*(10), 2608–2620.
610 https://doi.org/10.1016/J.NEUBIOREV.2013.08.010

611 Halder, T., Talwar, S., Jaiswal, A. K., & Banerjee, A. (2019). Quantitative Evaluation in
612 Estimating Sources Underlying Brain Oscillations Using Current Source Density Methods
613 and Beamformer Approaches. *Eneuro*, *6*(4), ENEURO.0170-19.2019.
614 https://doi.org/10.1523/eneuro.0170-19.2019

615 Han, S. W., & Marois, R. (2014). Functional fractionation of the stimulus-driven attention
616 network. *The Journal of Neuroscience : The Official Journal of the Society for*
617 *Neuroscience*, *34*(20), 6958–6969. https://doi.org/10.1523/JNEUROSCI.4975-13.2014

618 Huang, F., Tang, S., Sun, P., & Luo, J. (2018). Neural correlates of novelty and appropriateness
619 processing in externally induced constraint relaxation. *NeuroImage*, *172*, 381–389.
620 https://doi.org/10.1016/J.NEUROIMAGE.2018.01.070

621 Igelström, K. M., Webb, T. W., & Graziano, M. S. A. (2015). Neural Processes in the Human
622 Temporoparietal Cortex Separated by Localized Independent Component Analysis. *The*
623 *Journal of Neuroscience : The Official Journal of the Society for Neuroscience*, *35*(25),
624 9432–9445. https://doi.org/10.1523/JNEUROSCI.0551-15.2015
625 Janssen, T. W. P., Heslenfeld, D. J., van Mourik, R., Geladé, K., Maras, A., & Oosterlaan, J.
626 (2015). Alterations in the Ventral Attention Network During the Stop-Signal Task in
627 Children With ADHD: An Event-Related Potential Source Imaging Study. *Journal of*
628 *Attention Disorders*, 1087054715580847-. https://doi.org/10.1177/1087054715580847
629 Jensen, O., & Mazaheri, A. (2010). Shaping functional architecture by oscillatory alpha
630 activity: Gating by inhibition. *Frontiers in Human Neuroscience*, *4*.
631 https://doi.org/10.3389/fnhum.2010.00186
632 Karnath, H.-O. (2015). Spatial attention systems in spatial neglect. *Neuropsychologia*, *75*, 61–
633 73. https://doi.org/10.1016/j.neuropsychologia.2015.05.019
634 Klimesch, W. (2012, December). Alpha-band oscillations, attention, and controlled access to
635 stored information. *Trends in Cognitive Sciences*.
636 https://doi.org/10.1016/j.tics.2012.10.007
637 Krall, S. C., Rottschy, C., Oberwelland, E., Bzdok, D., Fox, P. T., Eickhoff, S. B., … Konrad,
638 K. (2015). The role of the right temporoparietal junction in attention and social interaction
639 as revealed by ALE meta-analysis. *Brain Structure and Function*, *220*(2), 587–604.
640 https://doi.org/10.1007/s00429-014-0803-z
641 Kubit, B., & Jack, A. I. (2013). Rethinking the role of the rTPJ in attention and social cognition
642 in light of the opposing domains hypothesis: findings from an ALE-based meta-analysis
643 and resting-state functional connectivity. *Frontiers in Human Neuroscience*, *7*, 323.
644 https://doi.org/10.3389/fnhum.2013.00323

645 Kulikowski, J. J., & Tolhurst, D. J. (1973). Psychophysical evidence for sustained and transient
646 detectors in human vision. *The Journal of Physiology*, *232*(1), 149–162.
647 https://doi.org/10.1113/jphysiol.1973.sp010261

648 Liu, Y., Bengson, J., Huang, H., Mangun, G. R., & Ding, M. (2014). Top-down Modulation of
649 Neural Activity in Anticipatory Visual Attention: Control Mechanisms Revealed by
650 Simultaneous EEG-fMRI. *Cerebral Cortex*, bhu204.
651 https://doi.org/10.1093/cercor/bhu204

652 Lynch, C. J. (2014). Towards a reconceptualization of the temporoparietal junction in stimulus-
653 driven attention. *The Journal of Neuroscience : The Official Journal of the Society for*
654 *Neuroscience*, *34*(40), 13277–13278. https://doi.org/10.1523/JNEUROSCI.2996-14.2014

655 Mars, R. B., Sallet, J., Schuffelgen, U., Jbabdi, S., Toni, I., & Rushworth, M. F. S. (2012).
656 Connectivity-Based Subdivisions of the Human Right "Temporoparietal Junction Area":
657 Evidence for Different Areas Participating in Different Cortical Networks. *Cerebral*
658 *Cortex*, *22*(8), 1894–1903. https://doi.org/10.1093/cercor/bhr268

659 Menon, V., & Uddin, L. Q. (2010). Saliency, switching, attention and control: a network model
660 of insula function. *Brain Structure & Function*, *214*(5–6), 655–667.
661 https://doi.org/10.1007/s00429-010-0262-0

662 Noonan, M. A. P., Adamian, N., Pike, A., Printzlau, F., Crittenden, B. M., & Stokes, M. G.
663 (2016). Distinct mechanisms for distractor suppression and target facilitation. *Journal of*
664 *Neuroscience*, *36*(6), 1797–1807. https://doi.org/10.1523/JNEUROSCI.2133-15.2016

665 Pascual-Marqui, R. D. (2007). Discrete, 3D distributed, linear imaging methods of electric
666 neuronal activity. Part 1: exact, zero error localization. Retrieved from
667 http://arxiv.org/abs/0710.3341

668 Pedrazzini, E., & Ptak, R. (2019). Damage to the right temporoparietal junction, but not lateral
669 prefrontal or insular cortex, amplifies the role of goal-directed attention. *Scientific*
670 *Reports*, *9*(1), 306. https://doi.org/10.1038/s41598-018-36537-3
671 Rennig, J., Himmelbach, M., Huberle, E., & Karnath, H.-O. (2015). Involvement of the TPJ
672 Area in Processing of Novel Global Forms. *Journal of Cognitive Neuroscience*, *27*(8),
673 1587–1600. https://doi.org/10.1162/jocn_a_00809
674 Schuwerk, T., Schurz, M., Müller, F., Rupprecht, R., & Sommer, M. (2017). The rTPJ's
675 overarching cognitive function in networks for attention and theory of mind. *Social*
676 *Cognitive and Affective Neuroscience*, *12*(1), 157–168.
677 https://doi.org/10.1093/scan/nsw163
678 Sokoliuk, R., Mayhew, S. D., Aquino, K. M., Wilson, R., Brookes, M. J., Francis, S. T., …
679 Mullinger, K. J. (2019). Two spatially distinct posterior alpha sources fulfill different
680 functional roles in attention. *The Journal of Neuroscience : The Official Journal of the*
681 *Society for Neuroscience*, 1993–18. https://doi.org/10.1523/JNEUROSCI.1993-18.2019
682 Stigliani, A., Jeska, B., & Grill-Spector, K. (2017). Encoding model of temporal processing in
683 human visual cortex. *Proceedings of the National Academy of Sciences of the United*
684 *States of America*, *114*(51), E11047–E11056. https://doi.org/10.1073/pnas.1704877114
685 Teichert, T., Grinband, J., & Ferrera, V. (2016). The importance of decision onset. *Journal of*
686 *Neurophysiology*, *115*(2), 643–661. https://doi.org/10.1152/jn.00274.2015
687 Van Essen, D. C. (2005). A Population-Average, Landmark-and Surface-based (PALS) atlas
688 of human cerebral cortex. https://doi.org/10.1016/j.neuroimage.2005.06.058
689 Vossel, S., Geng, J. J., & Fink, G. R. (2014). Dorsal and Ventral Attention Systems. *The*
690 *Neuroscientist*, *20*(2), 150–159. https://doi.org/10.1177/1073858413494269
691 Worden, M. S., Foxe, J. J., Wang, N., & Simpson, G. V. (2000). Anticipatory biasing of

692 visuospatial attention indexed by retinotopically specific alpha-band
693 electroencephalography increases over occipital cortex. *The Journal of Neuroscience : The Official Journal of the Society for Neuroscience*, *20*(6).
695 https://doi.org/10.1523/jneurosci.20-06-j0002.2000

696 Wöstmann, M., Alavash, M., & Obleser, J. (2019). Alpha oscillations in the human brain
697 implement distractor suppression independent of target selection. *The Journal of*
698 *Neuroscience*, 1954–19. https://doi.org/10.1523/jneurosci.1954-19.2019

699 Xia, M., Wang, J., & He, Y. (2013). BrainNet Viewer: A Network Visualization Tool for
700 Human Brain Connectomics. *PLoS ONE*, *8*(7).
701 https://doi.org/10.1371/journal.pone.0068910

702 Zumer, J. M., Scheeringa, R., Schoffelen, J.-M., Norris, D. G., & Jensen, O. (2014). Occipital
703 Alpha Activity during Stimulus Processing Gates the Information Flow to Object-
704 Selective Cortex. *PLoS Biology*, *12*(10), e1001965.
705 https://doi.org/10.1371/journal.pbio.1001965

706

707

708 **Legends, tables and figures**

709 **Table 1. Trial distribution across tasks.** The block-wise distribution of the Neutral Trials
710 (NT), Without Saliency Trials (WT) and Saliency Trials (ST) across the dynamic and the static
711 stimulus conditions have been listed.

712 **Table 2**. **Areas involved in processing saliency.** Coordinates of the regions of interests (ROIs)
713 of the reconstructed sources involved in saliency processing for a) dynamic stimulus condition
714 and b) static stimulus condition are listed.

Figure1. Experimental design. An example of the experimental paradigm used in the study illustrating the three different categories of trials: neutral trials (NT), without saliency trials (WT) and saliency trials (ST) is shown along with their presentation durations within a block which comprised of videos in the (A) Dynamic stimulus condition and static images in the (B) Static stimulus condition.

Figure 2. Behavior. The mean and standard error of the mean of neutral trials (NT), without saliency trials (WT) and saliency trials (ST) from all the nineteen participants are shown for the two task conditions: (A) Dynamic stimulus condition and (B) Static stimulus condition. The significant difference between any two categories of trials within a task condition was tested at 95% confidence interval using Wilcoxon ranksum test (*** represents $p<0.0001$ and ** represents $p=0.012$).

Figure 3. Power spectral density. The figure shows the grand-average of the power spectra of neutral trials (NT), without saliency trials (WT) and saliency trials (ST) across (A) Dynamic Stimulus condition and (B) Static Stimulus condition. The boxed regions represent those frequencies (alpha band, 8-11 Hz) which show a significant increase of power (ST>WT at $p=0.002$ and ST>NT at $p<0.0001$ in static stimulus condition; ST>WT at $p=0.04$ and ST>NT at $p=0.06$ in dynamic stimulus condition) in ST as compared to WT and NT, validated using Wilcoxon rank-sum test for individual frequency pairs within a condition. The left inset in each stimulus condition shows that the peak of alpha is at ~10 Hz for both (A) Dynamic Stimulus and (B) Static Stimulus. The right inset in each stimulus condition are topoplots highlighting the enhancement in alpha peak power (~10Hz) in ST with respect to WT across the sensor space computed using the alpha modulation index (AMI).

Figure 4. Source localization. The figure represents the cortical sources responsible for processing a salient distractor at the peak alpha frequency (~10 Hz) computed using the alpha

modulation index (AMI). The sources that were identified using eLORETA, a weighted minimum norm inverse solution, were the left and the right anterior temporo-parietal junction, the right posterior temporo-parietal junction, the right insula, the right lateral prefrontal cortex, the left and the right visual association areas for (A) Dynamic Stimulus; and the left and the right anterior temporo-parietal junction, the right insula, the right lateral prefrontal cortex (including the inferior frontal gyrus), the right visual association areas for (B) Static Stimulus. All the regions were approximated to the nearest Brodmann areas of the human brain.

Figure 5. Effective Connectivity. The figure represents the directional influences between the localized sources responsible for processing a salient distractor for (A) Dynamic Stimulus and (B) Static Stimulus. The arrows point from the driver node towards the effector node. The causalities were determined using a time-varying Granger Causality approach on the source reconstructed time-series data and the figure illustrates the top 50% of all the significant causations for each stimulus condition.

Table 1.

Trial information	Dynamic stimulus	Static stimulus
Total no. of blocks	8	8
No. of trials per block	70	30
NT	20	10
WT	20	10
ST	30*	10

*To reduce the drop in the pop-out effect of salient distractors due to habituation after multiple trial presentations, 3 kinds of salient distractors were used, varying in either color or size or both from the other moving dots. 10 trials each of an equisized red, a larger red and a larger

white dot were presented in a block as a salient distractor along with rest of the moving dots in ST.

Table 2.

a).

MNI coordinates of ROIs of dynamic stimulus				
x	*y*	*z*	*Brodmann area*	*ROI name*
45.5304	1.8176	7.6352	45	R. LPFC/IFG
49.0328	-67.0187	6.234	19	R. visual area
-43.0262	-44.5205	8.2927	40	L. ant. TPJ / SMG
-52.8281	-71.4317	0.9335	19	L. visual area
43.7931	-56.3395	28.768	39	R. post. TPJ / AG
47.7159	-14.6687	-0.9942	13	R. insula
47.8512	-30.7366	16.2046	40	R. ant. TPJ / SMG

b).

MNI coordinates of ROIs of static stimulus				
x	*y*	*z*	*Brodmann area*	*ROI name*
44.6437	-17.0274	13.1784	40	R. ant. TPJ / SMG
-40.6605	-32.5528	11.1861	40	L. ant. TPJ / SMG
45.2284	0.0653	-2.7002	13	R. insula
41.0606	15.3615	18.6218	9	R. LPFC
41.8174	-75.7257	-3.1578	19	R. visual area

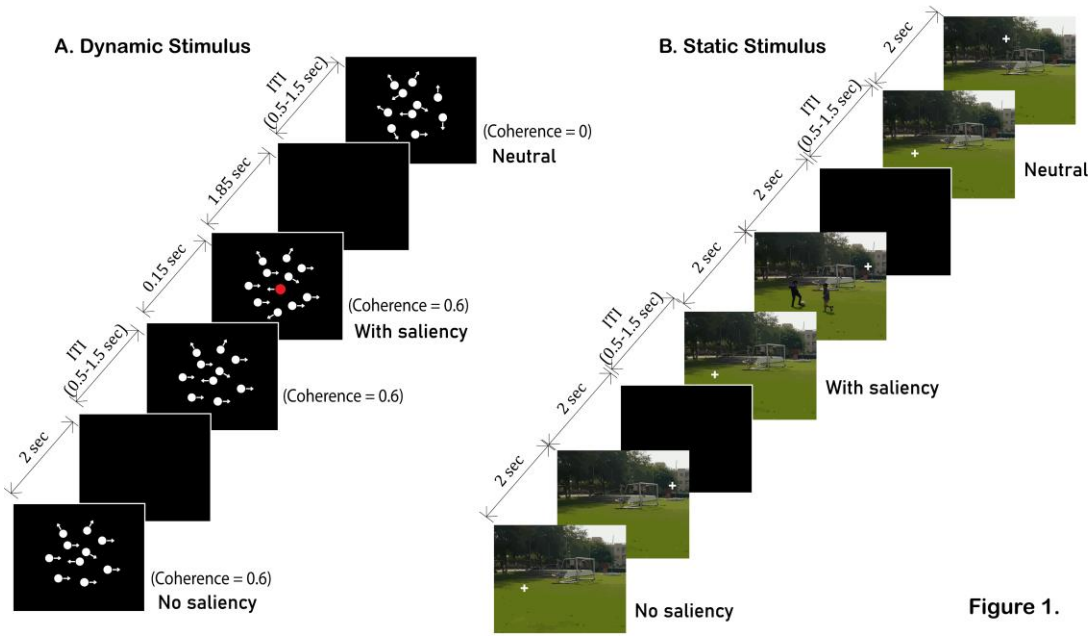

Figure 1.

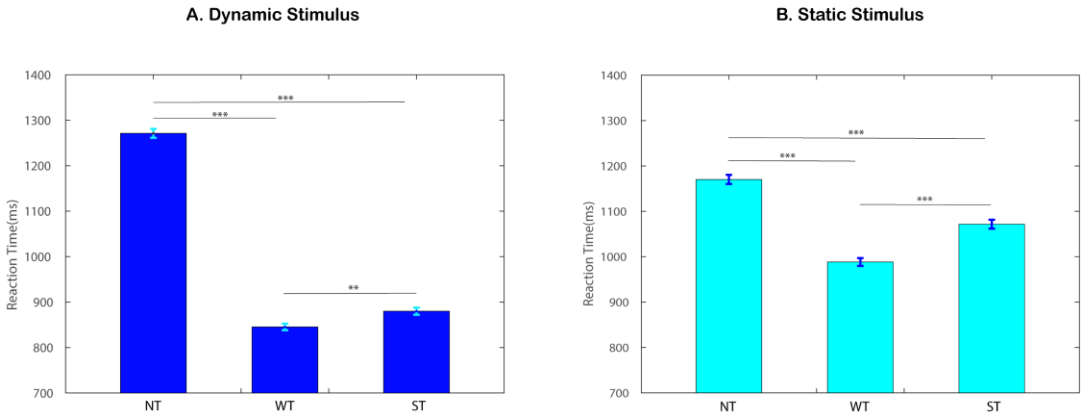

Figure 2.

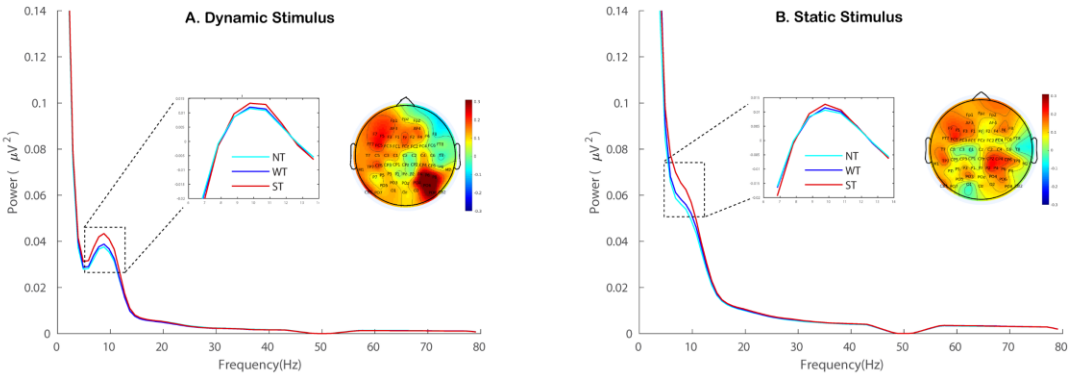

Figure 3.

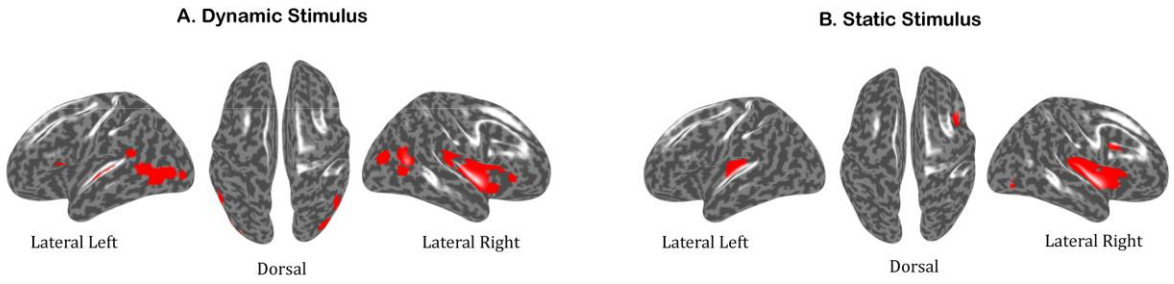

Figure 4.

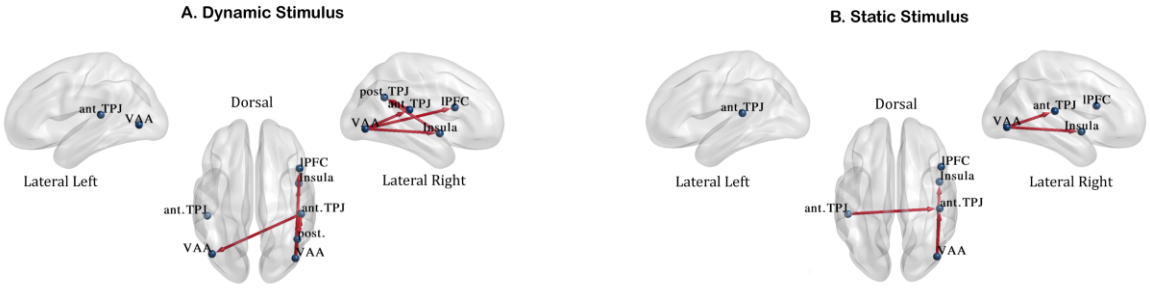

Figure 5.